Solar Energy Materials & Solar Cells 94 (2010) 128–132

Contents lists available at ScienceDirect

Solar Energy Materials & Solar Cells

journal homepage: www.elsevier.com/locate/solmat

Plasmon-enhanced optical absorption and photocurrent in organic bulk heterojunction photovoltaic devices using self-assembled layer of silver nanoparticles

Woo-Jun Yoon [a], Kyung-Young Jung [a,1], Jiwen Liu [b,2], Thirumalai Duraisamy [b,3], Rao Revur [b], Fernando L. Teixeira [a], Suvankar Sengupta [b], Paul R. Berger [a,c,*]

[a] Department of Electrical and Computer Engineering, Ohio State University, Columbus, OH 43210, USA
[b] MetaMateria Partners, 1275 Kinnear Road, Columbus, OH 43212, USA
[c] Department of Physics, Ohio State University, Columbus, OH 43210, USA

ARTICLE INFO

Article history:
Received 10 June 2009
Received in revised form
10 August 2009
Accepted 13 August 2009
Available online 9 September 2009

Keywords:
Ag nanoparticle
Surface plasmon
Solar cell
Photovoltaic
Organic bulk heterojunction

ABSTRACT

Improved optical absorption and photocurrent for polythiophene–fullerene bulk heterojunction photovoltaic devices is demonstrated using a unique self-assembled monolayer of Ag nanoparticles formed from a colloidal solution. With the presence of suitable nanoparticle organic capping groups that inhibit its propensity to agglomerate, the particle-to-particle spacing can be tailored. Transmission electron microscopy reveals the self-assembled Ag nanospheres are highly uniform with an average diameter of ~4 nm and controllable particle-to-particle spacing. The localized surface plasmon resonance peak is ~465 nm with a narrow full width at half maximum (95 nm). In the spectral range of 350–650 nm, where the organic bulk heterojunction photoactive film absorbs, an enhanced optical absorption is observed due to the increased electric field in the photoactive layer by excited localized surface plasmons within the Ag nanospheres. Under the short-circuit condition, the induced photocurrent efficiency (IPCE) measurement demonstrates that the maximum IPCE increased to ~51.6% at 500 nm for the experimental devices with the self-assembled layer of Ag nanoparticles, while the IPCE of the reference devices without the plasmon-active Ag nanoparticles is ~45.7% at 480 nm. For the experimental devices under air mass 1.5 global filtered illuminations with incident intensity of 100 mW/cm^2, the increased short-circuit current density is observed due to the enhancement of the photogeneration of excitons near the plasmon resonance of the Ag nanoparticles.

1. Introduction

Key advantages of organic photovoltaic (PV) technology are that organic based PV versus traditional inorganic semiconductors are inherently inexpensive; typically have very high optical absorption coefficients ($\geq 10^5\,cm^{-1}$); are compatible with large area and flexible substrates [1–3]; and can be fabricated using high-throughput low temperature processes for low-cost roll-to-roll manufacturing [4–7]. Although the efficiency of organic solar cells has improved to ~3–5% [8–10], the overall performance of organic solar cells is not yet high enough for commercial opportunities. In addition low stability and degradation of organic PV devices are required to be improved [11].

In order to improve the efficiency of organic solar cells, one approach, addressed in this paper, will be to yield increased optical absorption and photocurrent generation in the photoactive layer over a broad range of visible wavelengths by inducing surface plasmons through careful control of metallic nanoparticle's properties. It is well known that the optical absorption spectra of metal nanoparticles are dominated by surface plasmons [12]. With incident light, the surface charges of metallic nanoparticles interact with the electromagnetic field, leading to an electric field enhancement that can then be coupled to the photoactive absorption region. It has been extensively studied that surface plasmons can be tuned by changing the size, shape, particle material, substrates and overcoating of the metal particles [13–15].

* Corresponding author at: Department of Electrical and Computer Engineering, Ohio State University, 205 Dreese Laboratory, 2015 Neil Avenue, Columbus, OH 43210, USA. Tel.: +1 614 247 6235; fax: +1 614 292 7596.
E-mail address: pberger@ieee.org (P.R. Berger).
[1] Present address: Division of Electrical and Computer Engineering, Ajou University, Suwon 443-749, South Korea.
[2] Present address: Auld Technologies, 180 Outerbelt Street, Columbus, OH 43213, USA.
[3] Present address: Color and Glass Performance Materials, Ferro Corporation, 251 W Wylie Ave, Washington, PA 15301, USA.

0927-0248/$ - see front matter © 2009 Elsevier B.V. All rights reserved.
doi:10.1016/j.solmat.2009.08.006

The application of plasmonic materials to various PV devices has been widely utilized for improving the PV device performance [16–28]. Recently, Morfa et al. [21] reported an improved efficiency (η_{eff}) from ~1.3% to ~2.2% using surface plasmon-active Ag nanoparticle layers on indium-tin oxide (ITO) anode in poly(3-hexylthiophene) (P3HT) and phenyl-C_{61}-butyric-acid-methyl ester (PCBM) bulk heterojunction solar cell. In their study, an enhanced short-circuit current density (J_{sc}) is reported due to the increased optical absorption from surface plasmons. However, these Ag nanoparticles were actually random shapes formed during the early stages of electron-beam evaporation, forming a discontinuous Ag film of small islands with non-uniform diameters distributed on the ITO anode. As a result, their particle size and shape varied over a wide distribution which could distort the plasmonic effects by broadening their spectral enhancement [29]. Sundararajan et al. also showed that nanoparticle aggregates on the active area of the silicon diode can lead to suppression of photocurrent [30]. Yoon and Berger further showed that self-assembled Ag nanoparticles introduced a beneficial intermediate energy step which is between the anode electrode and the hole transporting layer to suppress phonon losses [31].

Recently various approaches to implementing a controlled surface plasmon-active Ag film onto organic solar cells have been introduced as random Ag nanohole films or periodic Ag nanocavity array [22,32]. However, it is still difficult to achieve controllable dimensions of nanoparticles (holes) size with a correspondingly tight distribution.

In this work, a unique colloidal Ag nanoparticle solution with the presence of suitable organic capping groups that stabilize the nanoparticles and inhibit their propensity to agglomerate is applied to organic bulk heterojunction PV devices. An improved optical absorption and photocurrent for PV devices is demonstrated due to the increased electric field in the photoactive layer by excited localized surface plasmons of Ag nanoparticles.

2. Experiments

The ITO-coated glass substrates were ultrasonicated in acetone and isopropyl alcohol, dried with nitrogen, and subsequently dried overnight in air before device fabrication. The substrates were next spin-cast using poly (3,4-ethylenedioxythiophene) poly (styrenesulfonate) (PEDOT:PSS) (Baytron® P, standard grade, HC Stark) after passing through a 0.45 μm filter. The substrates were then annealed at 140 °C for 10 min in air with a resulting thickness of 40 ± 2 nm. Thicknesses were each confirmed by ellipsometry and surface profilometry for PEDOT:PSS/Si and PEDOT:PSS/ITO/glass, respectively.

The colloid was prepared from an organic salt of Ag with toluene as the carrier liquid. The salt was decomposed under controlled condition resulting in formation of Ag nanoparticles. The nanoparticles were capped by carboxylic ligand. The Ag colloidal solution was then spin-cast atop the ITO-coated glass substrate. The substrates were then annealed at 140 °C for 10 min in air and then transferred into an inert glove box environment with ≤ 1 ppm level of oxygen and moisture for spin-casting of the photoactive layer.

The mixed solution consisting of poly(3-hexylthiophene) (P3HT) and [6,6]-Phenyl C61 butyric acid methyl ester (PCBM) in 1,2-dichlorobenzene was then spin-cast at 1000 rpm on the top of the self-assembled layer of Ag nanoparticles (AgNP), as described by Li et al. [8]. The mixed solution had a P3HT:PCBM weight ratio of a 1:1 with a concentration of 20 mg/ml (P3HT). The P3HT (Merck) with 94.5% regioregularity and PCBM (Nano-C) were used without further purification. The P3HT used here has a weight-average molecular weight (M_w) of 26,200 g/mol, corresponding to a number-average molecular weight (M_n) of 13,000 g/mol, and with a polydispersity (M_w/M_n) of ~2.

After spin-casting the photoactive layer, thermal annealing was then performed by directly placing the device on a digitally controlled hotplate at 110 °C for 10 min in an inert glove-box. The thickness of the photoactive film was ~160 nm. The devices were pumped down in vacuum (~10^{-7} Torr) and then the multilayer stack completed by the shadowmask evaporation of a Ca (25 nm)/Al (80 nm) cathode. The final composite device structure is ITO/PEDOT:PSS/AgNP/P3HT:PCBM/Ca/Al. In our experiments, control devices (ITO/PEDOT:PSS/P3HT:PCBM/Ca/Al) were also fabricated and tested without the self-assembled layer of Ag nanoparticles. Both sets of PV devices (control and experiment) were fabricated during the same batch processing. The active device area (A) was 0.01 cm^2.

The current density–voltage (J–V) measurements were performed with a semiconductor characterization system (Keithley 4200) at room temperature in air without any device encapsulation under the spectral output from a 150 W solar simulator (Newport) using an AM 1.5 G filter. The solar simulator was precisely calibrated to a KG5 color filtered silicon diode (Hamamatsu S1133) as the reference cell whose spectral response matches that of the testing cells as closely as possible in order to minimize any spectral mismatching factors [33]. The irradiance (100 mW/cm^2) of the solar simulator was adjusted using a reference cell that had been recently calibrated by the National Renewable Energy Laboratory (NREL). The induced photo-current efficiency (IPCE) was measured using a current preamplifier under short-circuit conditions after illuminating the devices with monochromatic light from a quartz-halogen lamp passing through a monochromator.

3. Results and discussions

For the colloidal Ag nanoparticle in toluene with a concentration of 0.5 wt% (Metamateria Partner), an average diameter of Ag nanoparticles was ~3.65 nm with a very high uniformly sized distribution profile of ~81%, determined by dynamic light scattering (Fig. 1a). The UV–vis spectrum of Ag nanoparticle solution shows a plasmon resonance peak at 412 nm with the full width at half maximum (FWHM) of ~61 nm, indicating the characteristics of Ag particles with a plasmon absorption band (Fig. 1b) [34].

Transmission electron microscopy (TEM) images indicate the self-assembled layer of Ag nanospheres with an average diameter of ~4 nm with uniform particle-to-particle spacing (Fig. 2a). In the X-ray photoelectron spectra, the Ag $3d_{5/2}$ peak is observed at 368.2 eV with a very narrow FHWM of 0.68 eV (not shown here), compared with elemental Ag (368.27 eV). The UV–vis spectrum of self-assembled layer of Ag nanoparticles shows the localized surface plasmon resonance peak at 465 nm with a FWHM of ~95 nm (Fig. 2b) [35].

Fig. 3 shows the optical density of P3HT:PCBM blend films with and without self-assembled layer of Ag nanoparticles with the red shoulder (at 602 nm), indicating effective self-organization of the regioregular P3HT [10]. In the spectral range of 350–650 nm where the P3HT:PCBM blend film is absorbing, the enhanced optical absorption was observed due to the increased electric field in the active photoactive layer by excited localized surface plasmons around the Ag nanospheres. This result corresponds to a ~16% increase of the total optical absorption of the devices in the spectral range of 350–650 nm.

The IPCE measurements for the control and experimental devices are shown in Fig. 4. Prior to the IPCE measurement, the spectral response of the color-filtered silicon solar cell

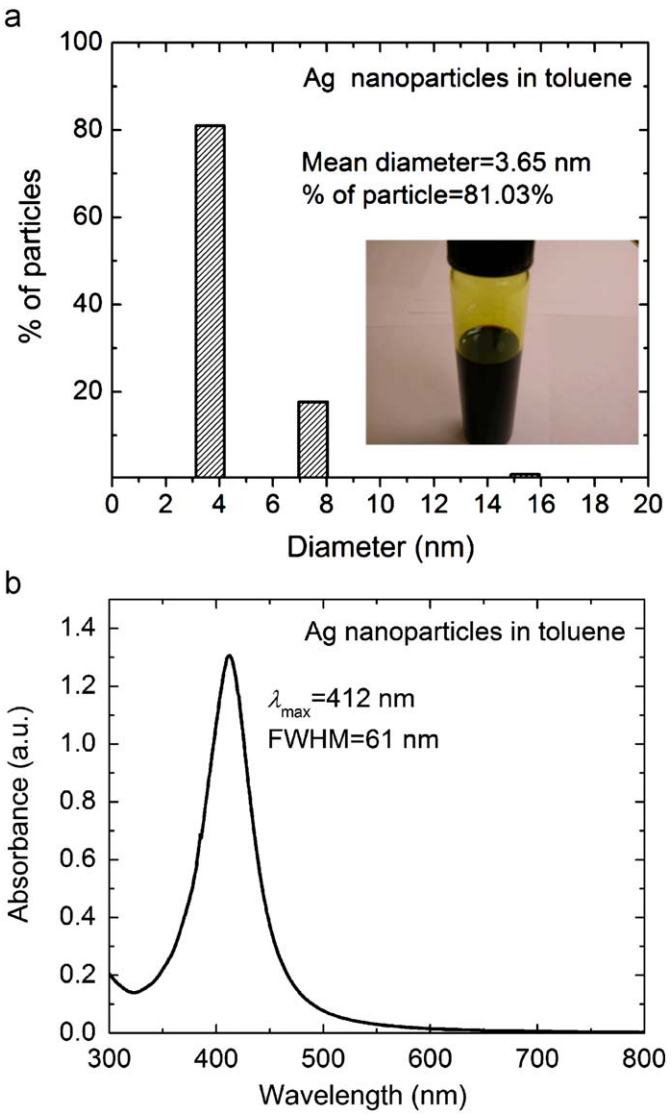

Fig. 1. (a) Particle size distribution of colloidal Ag nanoparticle with the concentration of 0.5 wt%. The average diameter of particles is ~3.65 nm with very high uniform size distribution profile of ~81%. The inset is the real image of the colloidal solution. (b) UV–vis absorption spectra of the diluted Ag colloidal solution showing a plasmon resonance at 412 nm with the FWHM of ~61 nm (the absorbance is baseline corrected with a background of toluene).

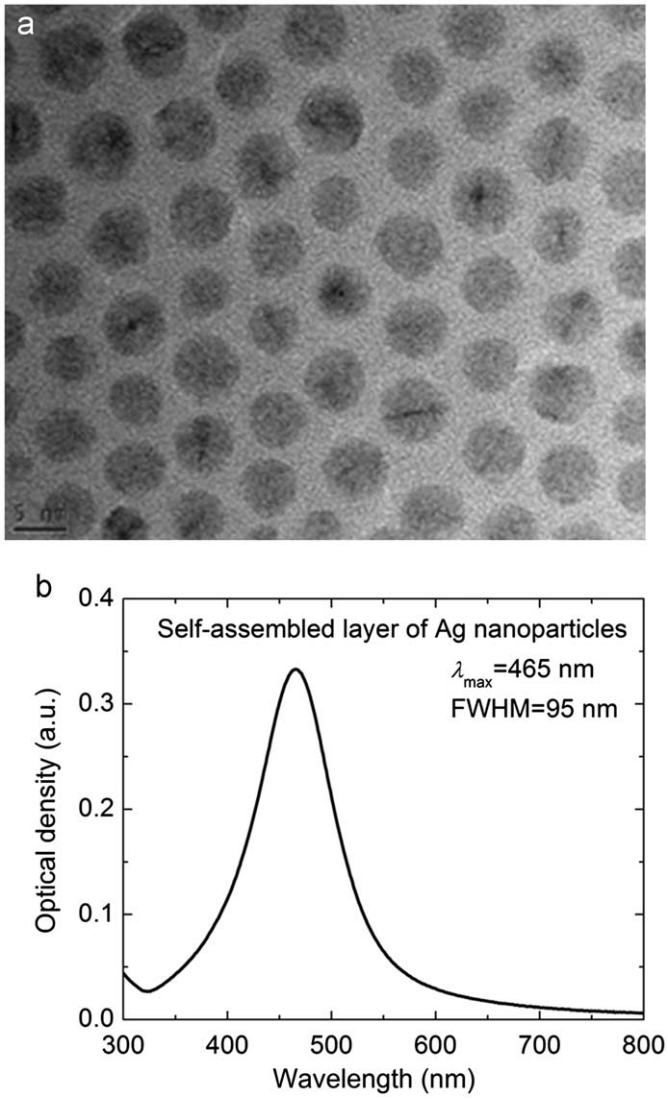

Fig. 2. (a) TEM image of the self-assembled Ag nanospheres layer with an average diameter of ~4 nm and with periodic particle-to-particle spacing. (b) UV–vis absorption spectra of the self-assembled layer of Ag nanoparticles (the absorbance is baseline corrected with a background of quartz substrate).

(Hamamatsu S1133) was measured and normalized to the NREL calibration result shown in the inset of Fig. 4. The IPCE of the control devices follows primarily the optical density of the P3HT:PCBM layer and the maximum IPCE was ~45.7% at 480 nm. With the presence of Ag nanoparticles in contact with the photoactive layer, the maximum IPCE was increased to ~51.6% at 500 nm. By integrating the product of this IPCE and the global reference solar spectrum, the calculated J_{sc} was ~6.8 mA/cm^2, while it was ~6.1 mA/cm^2 for the reference devices. With the presence of Ag nanoparticles in contact with the photoactive layer, an additional local photocurrent was created due to the enhancement of the photogeneration of excitons associated with enhanced electric field intensity from the localized surface plasmon resonance.

Fig. 5(a) shows J–V characteristics of both devices under dark. The control PV device exhibited a high current rectification ratio of $\sim 1 \times 10^5$ at ± 1 V, while it was only ~26 at ± 1 V for the experimental devices. This is indicative that the presence of self-assembled Ag nanoparticles on the PEDOT:PSS layer significantly shorted the electrical junction between the anode and the cathode. The highly elevated reverse saturation current for the experiment samples suggests that the Ag nanoparticles significantly introduced surface recombination centers, leading to a higher leakage current density in the experimental devices for $V < 0.5$ V.

Under AM 1.5 G filtered illuminations for a calibrated solar simulator with an overall intensity of 100 mW/cm^2, the control device (ITO/PEDOT:PSS/P3HT:PCBM/Ca/Al) exhibited an η_{eff} of ~2.2% with a high fill factor (FF) of ~64%. The open-circuit voltage (V_{oc}) and the J_{sc} of the control devices were ~0.56 V and ~6.2 mA/cm^2, respectively. For the experimental devices incorporating the self-assembled Ag nanoparticle layer between the PEDOT:PSS and P3HT:PCBM, an η_{eff} of 1.2% with $V_{oc} = 0.42$ V, J_{sc}~7.0 mA/cm^2 and FF ~35% were measured. For experimental devices, the increased J_{sc} was observed due to the enhancement of the photogeneration of excitons near the plasmon resonance and into the red, as shown in Fig. 4. The measured J_{sc} here also matches closely the J_{sc} calculated from the IPCE measurement (J_{sc}~6.9 mA/cm^2). However, the specific series resistance (R_sA), defined by the slope of the J–V curve at $J = 0$ mA/cm^2 is estimated to be about ~48.1 Ω

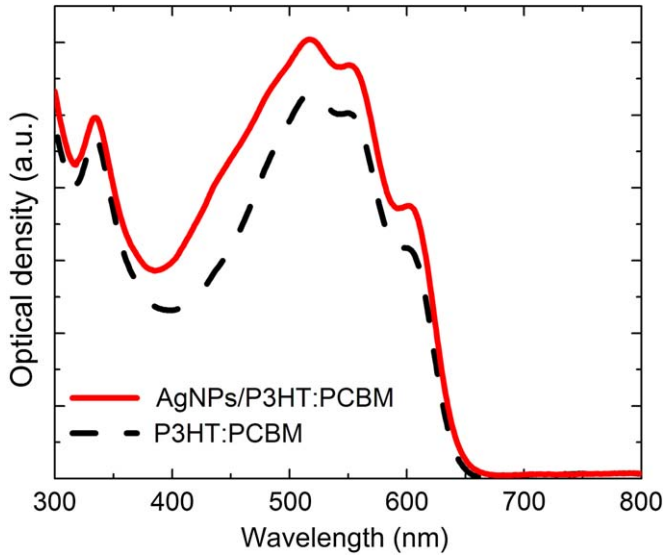

Fig. 3. The optical absorption spectra of the P3HT:PCBM bulk heterojunction with and without self-assembled layer of Ag nanoparticles (the absorbance is baseline corrected with a background of PEDOT:PSS/quartz substrate).

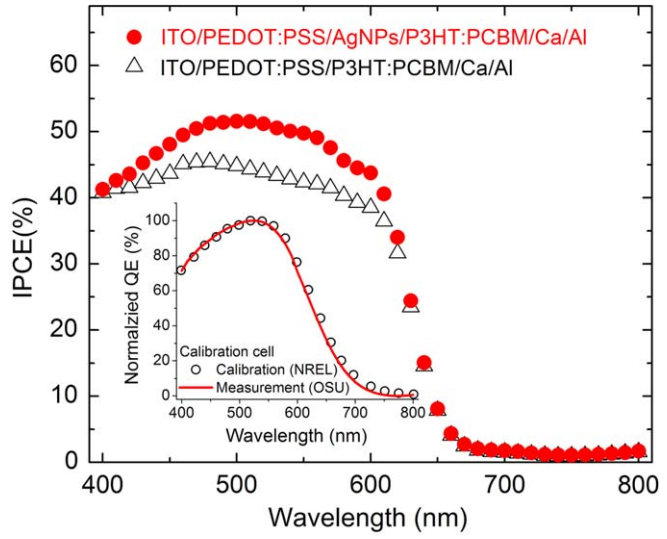

Fig. 4. IPCE measurement of the control device (ITO/PEDOT:PSS/P3HT:PCBM/Ca/Al) and the experimental device (ITO/PEDOT:PSS/Ag nanoparticles (AgNPs)/P3HT:PCBM/Ca/Al). The inset is the spectral response of the color-filtered silicon solar cell (Hamamatsu S1133) measured in the lab and then normalized to the NREL calibration data.

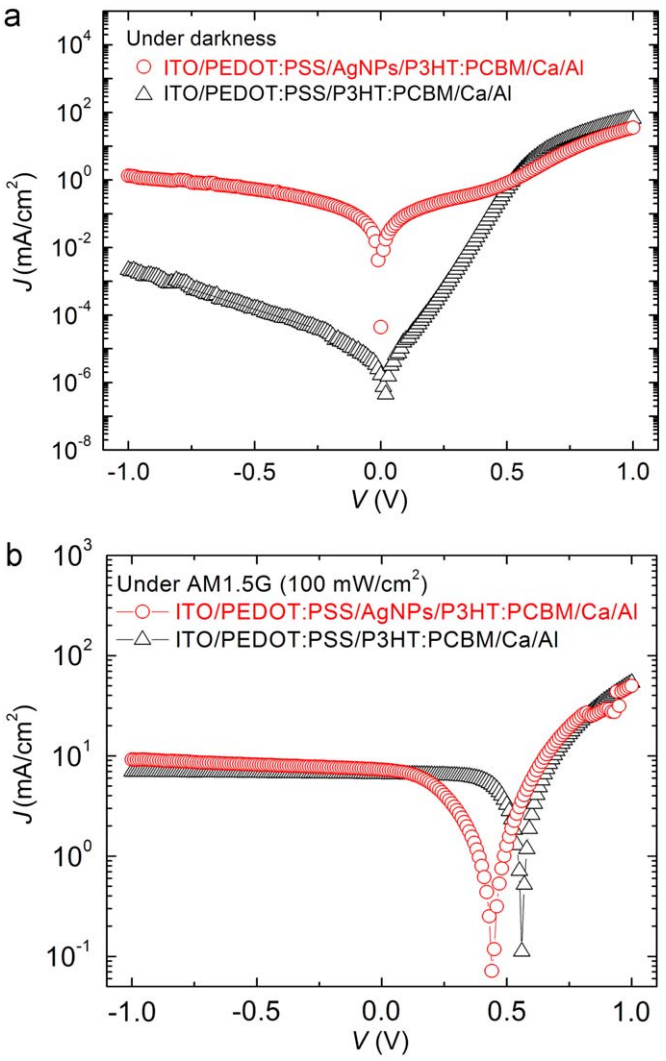

Fig. 5. (a) *J–V* characteristics of the control device (ITO/PEDOT:PSS/P3HT:PCBM/Ca/Al) and the experimental device (ITO/PEDOT:PSS/Ag nanoparticles (AgNPs)/P3HT:PCBM/Ca/Al) in darkness. (b) The corresponding *J–V* characteristics under AM 1.5 G filtered spectral illumination at an incident intensity of 100 mW/cm^2.

Table 1
Parameters for the control and experimental PV devices under AM 1.5 G filtered spectral illumination at an incident intensity of 100 mW/cm^2.

	J_{sc} (mA/cm^2)	V_{oc} (V)	FF (%)	η_{eff} (%)	R_{sh} (kΩ)	R_sA (Ω cm^2)
Control	6.2±0.13	0.56±0.01	64±1.8	2.2±0.23	98±39	13.3±1.8
Experimental	7.0±0.15	0.42±0.03	35±1.4	1.2±0.07	24±5	48.1±5.9

cm^2 (for experimental devices), increased by more than a factor of three compared with the control devices (~13.3 Ω cm^2) [36]. Due to the combination of elevated series resistance and lowered shunt resistance, the FF in the experimental devices significantly decreased to ~35%. Although the fabrication conditions for both the P3HT:PCBM blend film and cathode deposition were held constant in this work, V_{oc} decreased in the experimental devices. This lowered V_{oc} could be due to the higher surface recombination at the interface between the self-assembled layer of Ag nanoparticles and the P3HT:PCBM film. Parameters for the control and experimental PV devices under AM 1.5 G filtered spectral illumination at an incident intensity of 100 mW/cm^2 are summarized in Table 1.

When the Ag nanoparticles are formed instead between the ITO and PEDOT:PSS (ITO/Ag nanoparticles/PEDOT:PSS/P3HT:PCBM/Ca/Al), the photocurrent enhancement was not observed while recorded V_{oc} and FF are ~0.56 V and ~41%, respectively. This could be attributed to the exponential decay of the electrical field by excited surface plasmons of Ag nanoparticles in the PEDOT:PSS layer. The surface recombination at Ag nanoparticles could be significantly reduced by placing the Ag nanoparticles under the PEDOT:PSS layer. Further optimization of the plasmon-enhanced organic bulk heterojunction is underway.

Further optimization of the plasmon-enhanced organic bulk heterojunction can be achieved by tailoring geometrical parameters such as the size and shape of nanoparticles. This optimization is currently in progress by extending the

finite-difference time-domain method [37] to Drude dispersion models [38,39] and the periodic boundary condition.

4. Conclusions

In conclusion, we have shown an enhanced optical absorption and improved J_{sc} for polymer–fullerene bulk heterojunction PV devices, mainly due to the localized surface plasmon-enhanced photogeneration of excitons through the usage of plasmon-active Ag nanospheres between the PEDOT:PSS and the photoactive layer. Although the measured J_{sc} was increased, significant V_{oc} and FF losses were observed. Considering the enhanced saturation current from their J–V curves under darkness, the Ag nanoparticles considerably increased the surface recombination at the interface between PEDOT:PSS and P3HT:PCBM. The self-assembled layer of Ag nanoparticles also acts as the energy barrier for the charge extraction and injection, based on the increased series resistance of the devices.

Acknowledgements

The authors would like to thank Paul Ciszek and Keith Emery at the National Renewable Energy Lab (NREL) for calibration and very helpful discussions, Prof. Malcolm H. Chisholm, Dr. Yagnaseni Ghosh, Lynetta M. Mier and Prof. Terry L. Gustafson for optical measurements, Dr.Yun Wu and Dr. Robert J. Davis for dynamic light scattering measurement, Dr. Lisa Hommel for XPS measurement and James Jones for help with equipment maintenance. This work was supported by the Wright Center for Photovoltaics Innovation and Commercialization (PVIC) and the Institute for Materials Research (IMR).

References

[1] C. Lungenschmied, G. Dennler, H. Neugebauer, S.N. Sariciftci, M. Glatthaar, T. Meyer, A. Meyer, Flexible, long-lived, large-area, organic solar cells, Sol. Energy Mater. Sol. Cells 91 (2007) 379–384.
[2] F.C. Krebs, M. Jørgensen, K. Norrman, O. Hagemann, J. Alstrup, T.D. Nielsen, J. Fyenbo, K. Larsen, J. Kristensen, A complete process for production of flexible large area polymer solar cells entirely using screen printing—first public demonstration, Sol. Energy Mater. Sol. Cells 93 (2009) 422–441.
[3] R. Tipnis, J. Bernkopf, S. Jia, J. Krieg, S. Li, M. Storch, D. Laird, Large-area organic photovoltaic module—fabrication and performance, Sol. Energy Mater. Solar Cells 93 (2009) 442–446.
[4] C.J. Brabec, N.S. Sariciftci, J.C. Hummelen, Plastic solar cells, Adv. Funct. Mater. 11 (2001) 15–26.
[5] F.C. Krebs, S.A. Gevorgyan, J. Alstrup, A roll-to-roll process to flexible polymer solar cells: model studies, manufacture and operational stability studies, J. Mater. Chem. 19 (2009) 5442–5451.
[6] L. Blankenburg, K. Schultheis, H. Schache, S. Sensfuss, M. Schröner, Reel-to-reel wet coating as an efficient up-scaling technique for the production of bulk-heterojunction polymer solar cells, Sol. Energy Mater. Sol. Cells 93 (2009) 476–483.
[7] F.C. Krebs, Fabrication and processing of polymer solar cells: a review of printing and coating techniques, Sol. Energy Mater. Sol. Cells 93 (2009) 394–412.
[8] G. Li, V. Shrotriya, J. Huang, Y. Yao, T. Moriarty, K. Emery, Y. Yang, High-efficiency solution processable polymer photovoltaic cells by self-organization of polymer blends, Nat. Mater. 4 (2005) 864–868.
[9] W.L. Ma, C.Y. Yang, X. Gong, K. Lee, A.J. Heeger, Thermally stable efficient polymer solar cells with nanoscale control of the interpenetrating network morphology, Adv. Funct. Mater. 15 (2005) 1617–1622.
[10] Y. Kim, S. Cook, S.M. Tuladhar, S.A. Choulis, J. Nelson, J.R. Durrant, D.D.C. Bradley, M. Giles, I. McCulloch, C.-S. Ha, M. Ree, A strong regioregularity effect in self-organizing conjugated polymer films and high-efficiency polythiophene: fullerene solar cells, Nat. Mater. 5 (2006) 197–203.
[11] M. Jøgensen, K. Norrman, F.C. Krebs, Stability/degradation of polymer solar cells, Sol. Energy Mater. Sol. Cells 92 (2008) 686–714.
[12] W.L. Barnes, A. Dereux, T.W. Ebbesen, Surface plasmon subwavelength optics, Nature 424 (2003) 824–830.
[13] J.J. Mock, M. Barbic, D.R. Smith, D.A. Schultz, S. Schultz, Shape effects in plasmon resonance of individual colloidal silver nanoparticles, J. Chem. Phys. 116 (2002) 6755–6759.
[14] P. Royer, J.P. Goudonnet, R.J. Warmack, T.L. Ferrell, Substrate effects on surface-plasmon spectra in metal-island films, Phys. Rev. B 35 (1987) 3753–3759.
[15] G. Xu, M. Tazawa, P. Jin, S. Nakao, K. Yoshimura, Wavelength tuning of surface plasmon resonance using dielectric layers on silver island films, Appl. Phys. Lett. 82 (2003) 3811–3813.
[16] S. Hayashi, K. Kozaru, K. Yamamoto, Enhancement of photoelectric conversion efficiency by surface plasmon excitation: a test with an organic solar cell, Solid State Commun. 79 (1991) 763–767.
[17] O. Stenzel, A. Stendal, K. Voigtsberger, C. von Borczyskowski, Enhancement of the photovoltaic conversion efficiency of copper phthalocyanine thin film devices by incorporation of metal clusters, Sol. Energy Mater. Sol. Cells 37 (1995) 337–348.
[18] R.C. Joseph, N.J. Halas, Optimized plasmonic nanoparticle distributions for solar spectrum harvesting, Appl. Phys. Lett. 89 (2006) 153120.
[19] J.K. Mapel, M. Singh, M.A. Baldo, K. Celebi, Plasmonic excitation of organic double heterostructure solar cells, Appl. Phys. Lett. 90 (2007) 121102.
[20] S. Pillai, K.R. Catchpole, T. Trupke, M.A. Green, Surface plasmon enhanced silicon solar cells, J. Appl. Phys. 101 (2007) 093105.
[21] A.J. Morfa, K.L. Rowlen, T.H. Reilly III, M.J. Romero, J.v.d. Lagemaat, Plasmon-enhanced solar energy conversion in organic bulk heterojunction photovoltaics, Appl. Phys. Lett. 92 (2008) 013504.
[22] T.H. Reilly III, J. van der Lagemaat, R.C. Tenent, A.J. Morfa, K.L. Rowlen, Surface-plasmon enhanced transparent electrodes in organic photovoltaics, Appl. Phys. Lett. 92 (2008) 243304.
[23] J. Bellessa, C. Bonnand, J.C. Plenet, J. Mugnier, Strong coupling between surface plasmons and excitons in an organic semiconductor, Phys. Rev. Lett. 93 (2004) 036404.
[24] H. Carl, Z. Michael, K. Bengt, Enhanced charge carrier generation in dye sensitized solar cells by nanoparticle plasmons, Appl. Phys. Lett. 92 (2008) 013113.
[25] R.B. Konda, R. Mundle, H. Mustafa, O. Bamiduro, A.K. Pradhan, U.N. Roy, Y. Cui, A. Burger, Surface plasmon excitation via Au nanoparticles in n-CdSe/p-Si heterojunction diodes, Appl. Phys. Lett. 91 (2007) 191111.
[26] M. Westphalen, U. Kreibig, J. Rostalski, H. Lüth, D. Meissner, Metal cluster enhanced organic solar cells, Sol. Energy Mater. Sol. Cells 61 (2000) 97–105.
[27] W.-J. Yoon, P.R. Berger, 4.8% efficient poly(3-hexylthiophene)–fullerene derivative (1:0.8) bulk heterojunction photovoltaic devices with plasma treated AgO_x/indium tin oxide anode modification, Appl. Phys. Lett. 92 (2008) 013306.
[28] K.R. Catchpole, A. Polman, Plasmonic solar cells, Opt. Express 16 (2008) 21793–21800.
[29] I.O. Sosa, C. Noguez, R.G. Barrera, Optical properties of metal nanoparticles with arbitrary shapes, J. Phys. Chem. B 107 (2003) 6269–6275.
[30] S.P. Sundararajan, N.K. Grady, N. Mirin, N.J. Halas, Nanoparticle-induced enhancement and suppression of photocurrent in a silicon photodiode, Nano Letters 8 (2008) 624–630.
[31] W.-J. Yoon, P.R. Berger, Surface modifications to the indium tin oxide (ITO) anodes through plasma oxidized silver for efficient poly(3-hexylthiophene)–fullerene derivative (1:0.8) bulk heterojunction photovoltaic devices, in: Thirty IEEE Photovoltaic Specialists Conference, San Diego, CA, 2008.
[32] C.L. Nathan, A.L. Wade, O. Sang-Hyun, J.H. Russell, Plasmonic nanocavity arrays for enhanced efficiency in organic photovoltaic cells, Appl. Phys. Lett. 93 (2008) 123308.
[33] V. Shrotriya, G. Li, Y. Yao, T. Moriarty, K. Emery, Y. Yang, Accurate measurement and characterization of organic solar cells, Adv. Funct. Mater. 16 (2006) 2016–2023.
[34] A. Taleb, C. Petit, M.P. Pileni, Synthesis of highly monodisperse silver nanoparticles from AOT reverse micelles: a way to 2D and 3D self-organization, Chem. Mater. 9 (1997) 950–959.
[35] A. Taleb, C. Petit, M.P. Pileni, Optical properties of self-assembled 2D and 3D superlattices of silver nanoparticles, J. Phys. Chem. B 102 (1998) 2214–2220.
[36] S.K. Hau, H.-L. Yip, K. Leong, A.K.Y. Jen, Spraycoating of silver nanoparticle electrodes for inverted polymer solar cells, Org. Electron. 10 (2009) 719–723.
[37] A. Taflove, S.C. Hagness, Computational Electrodynamics: The Finite-Difference Time-Domain Method, third ed., Artech House, Norwood, MA, 2005.
[38] K.-Y. Jung, F.L. Teixeira, R.M. Reano, Au/SiO_2 nanoring plasmon waveguides at optical communication band, J. Lightwave Technol. 25 (2007) 2757–2765.
[39] K.-Y. Jung, F.L. Teixeira, Multispecies ADI-FDTD algorithm for nanoscale three-dimensional photonic metallic structures, IEEE Photon. Technol. Lett. 19 (2007) 586–588.